

# Particle production in Pb+Pb collisions at the CERN-SPS

I.G. Bearden,<sup>1</sup> H. Bøggild,<sup>1</sup> J. Boissevain,<sup>2</sup> P.H.L. Christiansen,<sup>1</sup> L. Conin,<sup>3</sup> J. Dodd,<sup>4</sup> B. Erasmus,<sup>3</sup> S. Esumi,<sup>5,\*</sup> C.W. Fabjan,<sup>6</sup> D. Ferenc,<sup>7,†</sup> D.E. Fields,<sup>2,‡</sup> A. Franz,<sup>6,§</sup> J.J. Gaardhøje,<sup>1</sup> M. Hamelin,<sup>8</sup> A.G. Hansen,<sup>1,¶</sup> O. Hansen,<sup>1</sup> D. Hardtke,<sup>9,\*\*</sup> H. van Hecke,<sup>2</sup> E.B. Holzer,<sup>6</sup> T.J. Humanic,<sup>9</sup> P. Hummel,<sup>6</sup> B.V. Jacak,<sup>10</sup> K. Kaimi,<sup>11,††</sup> M. Kaneta,<sup>11,\*\*</sup> T. Kohama,<sup>11</sup> M. Kopytine,<sup>10,‡‡</sup> M. Leltchouk,<sup>3</sup> A. Ljubičić, Jr.,<sup>7,§</sup> B. Lörstad,<sup>12</sup> N. Maeda,<sup>11</sup> R. Malina,<sup>6</sup> L. Martin,<sup>3</sup> A. Medvedev,<sup>4</sup> M. Murray,<sup>8</sup> H. Ohnishi,<sup>11,§§</sup> G. Paic,<sup>6,9</sup> S.U. Pandey,<sup>6</sup> F. Piuz,<sup>6</sup> J. Pluta,<sup>3,¶¶</sup> V. Polychronakos,<sup>13</sup> M. Potekhin,<sup>4</sup> G. Poulard,<sup>6</sup> D. Reichhold,<sup>9,\*\*\*</sup> A. Sakaguchi,<sup>11,†††</sup> J. Schmidt-Sørensen,<sup>12</sup> J. Simon-Gillo,<sup>2,‡‡‡</sup> W. Sondheim,<sup>2</sup> M. Spiegel,<sup>6</sup> T. Sugitate,<sup>11</sup> J.P. Sullivan,<sup>2</sup> Y. Sumi,<sup>11,§§§</sup> W.J. Willis,<sup>4</sup> K.L. Wolf,<sup>8,††</sup> N. Xu,<sup>2,\*\*</sup> and D.S. Zachary<sup>9</sup>

(NA44 collaboration)

<sup>1</sup>Niels Bohr Institute, DK-2100, Copenhagen, Denmark

<sup>2</sup>Los Alamos National Laboratory, Los Alamos, New Mexico 87545

<sup>3</sup>Nuclear Physics Laboratory of Nantes, 44072 Nantes, France

<sup>4</sup>Columbia University, New York, New York 10027

<sup>5</sup>Hiroshima University, Higashihiroshima, Hiroshima 739-8526, Japan

<sup>6</sup>CERN, CH-1211 Geneva 23, Switzerland

<sup>7</sup>Rudjer Bošković Institute, Zagreb, Croatia

<sup>8</sup>Cyclotron Institute, Texas A&M University, College Station, Texas 77843

<sup>9</sup>Ohio State University, Columbus, Ohio 43210

<sup>10</sup>State University of New York, Stony Brook, New York 11794

<sup>11</sup>Hiroshima University, Higashi-Hiroshima 739-8526, Japan

<sup>12</sup>University of Lund, S-22362 Lund, Sweden

<sup>13</sup>Brookhaven National Laboratory, Upton, New York 11973

(Dated: February 9, 2020)

The NA44 experiment has measured single particle inclusive spectra for charged pions, kaons, and protons as a function of transverse mass near mid-rapidity in 158 A GeV/c Pb+Pb collisions. From the particle mass dependence of the observed  $m_T$  distributions, we are able to deduce a value of about 120 MeV for the temperature at thermal freeze-out. From the observed ratios of the rapidity densities, we find values of the chemical potentials for light and strange quarks and a chemical freeze-out temperature of approximately 140 MeV.

PACS numbers: 25.75.-q,13.85.-t,25.40.Ve

## I. INTRODUCTION

The goal of heavy ion collision research at ultra-relativistic energies is to understand the fundamental properties of nuclear matter under extreme conditions of high particle and energy density. When these den-

sities are sufficient, quarks should no longer be confined in hadrons but instead move freely through the entire volume. The colliding system expands and cools, driven by the large internal pressure generated by the strong interaction of the constituents. The quarks eventually become confined again, forming hadrons that are later detected by experiments. The hadron yields and momentum distributions provide information about the temperature, density, and dynamics of the latter stages of the collision. This allows inference of conditions at a relatively early stage of the collisions.

The multiplicity of the produced hadrons ranges from several hundred to a few thousand in relativistic heavy ion collisions, and their rapidity density cannot be explained by simple superposition of  $p+p$  collisions. Consequently, final state rescattering may play an important role. The transverse momentum distributions of the hadrons display a Boltzmann-like shape, inspiring a thermodynamical interpretation of the momentum distributions.

In this report, we present invariant cross sections of  $\pi^\pm$ ,  $K^\pm$ ,  $p$ , and  $\bar{p}$ , as a function of transverse mass near mid-rapidity in central 158 A GeV/c Pb+Pb collisions. NA44 has previously reported the particle yields for pi-

\*Now at Univ. of Tsukuba, Tsukuba, Ibaraki 305-8571, Japan

†Now at Univ. of California, Davis, CA 95616

‡Now at Univ. of New Mexico, Albuquerque, NM 87185

§Now at BNL, Upton, NY 11973

¶Now at LANL, Los Alamos, NM 87545

\*\*Now at LBNL, Berkeley, CA 94720

††Deceased

‡‡On unpaid leave from P.N.Lebedev Physical Institute, Russian Academy of Sciences; Now at Kent State Univ., Kent, OH 44242

§§Now at RIKEN, Wako, Saitama 351-0198, Japan

¶¶Now at Institute of Physics, Warsaw Univ. of Technology, Koszykowa 75,00-662, Warsaw, Poland

\*\*\*Now at Creighton Univ., Omaha, NE 68178

†††Now at Osaka Univ., Toyonaka, Osaka 560-0043, Japan

‡‡‡Now at U.S. Department of Energy, Germantown, MD, 20874-1290

§§§Now at Hiroshima International Univ., Kamo 724-0695, Japan

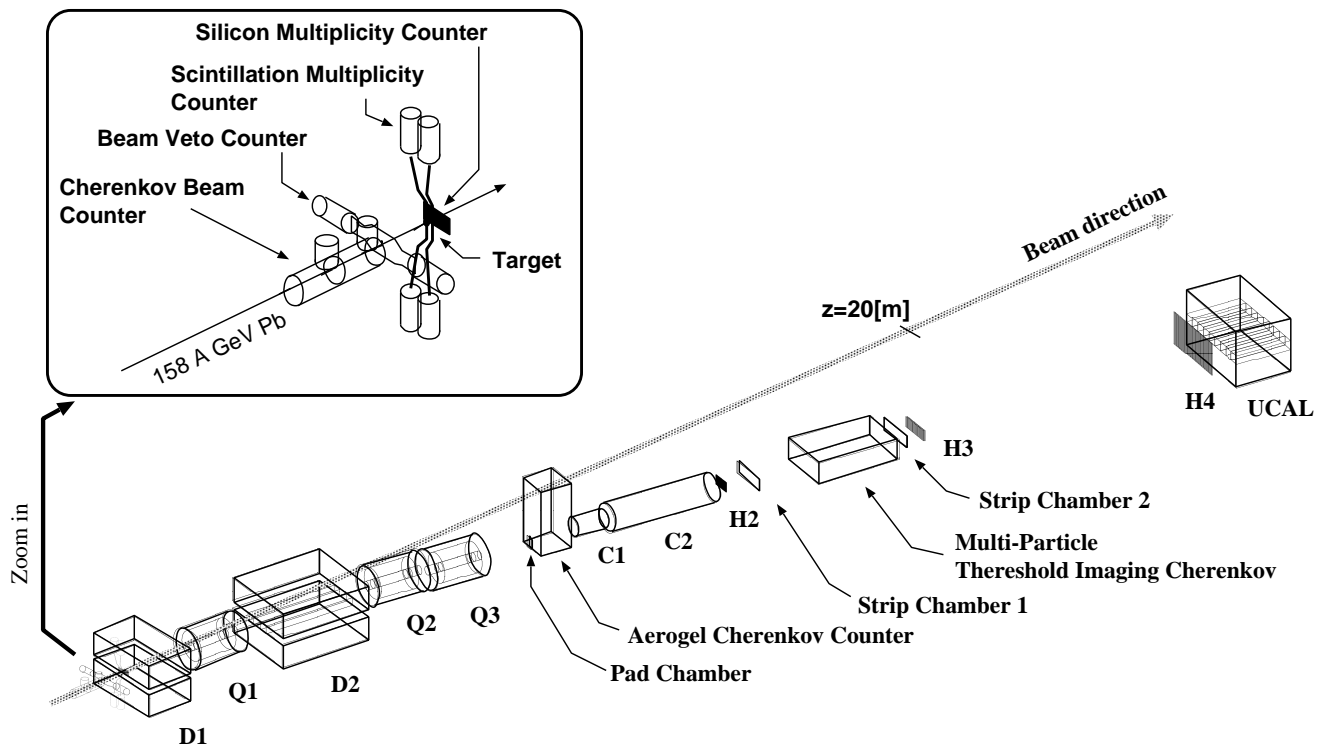


FIG. 1: The schematic view of NA44 spectrometer.

ons, kaons, and protons in  $p+A$  to  $S+A$  collisions [1, 2], kaon production in  $Pb+Pb$  [3], and anti-proton and anti-deuteron production in  $Pb+Pb$  [4]. Because of the excellent particle identification and systematic measurements from small to large systems, NA44 is well-suited to study the thermal and chemical properties of the hadronic system at freeze-out. The dependence of the thermal parameters on the colliding system size will also be discussed.

## II. NA44 EXPERIMENT

The NA44 focusing spectrometer is designed to measure one and two particle momentum distribution of charged hadrons near mid-rapidity [5]. A schematic view of the spectrometer is shown in Fig. 1. The target was a lead disk of 2 mm thickness (3.4% interaction probability for  $Pb+Pb$ ). A Cherenkov gas beam counter (CX) [6] and a beam veto counter (CX-veto) were placed upstream of the target. CX selects single beam particles up to a rate of  $2 \times 10^6$  ions/second while the CX-veto signals the presence of any beam halo. A scintillation multiplicity counter (T0) is 10 mm downstream of the target, and produces a pulse height proportional to the number of charged particles impinging upon it. T0 covers 20% of the azimuthal angle and has a pseudo-rapidity range of  $0.6 \leq \eta \leq 3.3$ . This contains mid-rapidity ( $y_{mid} = 2.9$ ) for the  $Pb+Pb$  collision. T0 is used to select collision centrality at the trigger level.

Two dipole magnets (D1 and D2) analyze the particle momenta. Three super-conducting quadrupole magnets help focus the particles. The PID/tracking detectors measure hit positions after the magnetic analysis, and consist of strip chambers and scintillation hodoscopes, along with two threshold gas Cherenkov counters, C1 and C2. Three hodoscopes, H2, H3, and H4 consist of 60, 50, and 60 scintillation counters, respectively. Only H2 and H3 were used in this analysis. The hodoscopes provide position information for tracking, with vertical hit information determined from photomultiplier tubes on each end of every counter. The hodoscopes also measure time-of-flight for hadron identification [7]. One pad chamber (PC) and two strip chambers (SC1 and SC2) provide 0.3 mm position resolution for track reconstruction. C1 and C2 contain Freon 12 at 2.7 atm and  $N_2$  at 1.3 atm respectively, and identify particles at the trigger level. The trigger requires a valid beam, a high multiplicity detected in T0 (central collision), at least one track in each hodoscope, and absence of a veto particle such as electron or pion for  $K/p$  runs ( $e/\pi$  veto).

The timing signal from CX is used for the time-of-flight (TOF) start with a resolution of 35 ps. The average of the top and bottom PMT of the hodoscope was used for the stop signal. The overall TOF resolution was approximately 100 ps and 80 ps for H2 and H3, respectively.

Two magnetic field settings of the spectrometer were used, yielding nominal momentum of 4 GeV/c ( $3.2 \leq p \leq 5.2$  GeV/c) and 8 GeV/c ( $6.0 \leq p \leq 9.8$  GeV/c).

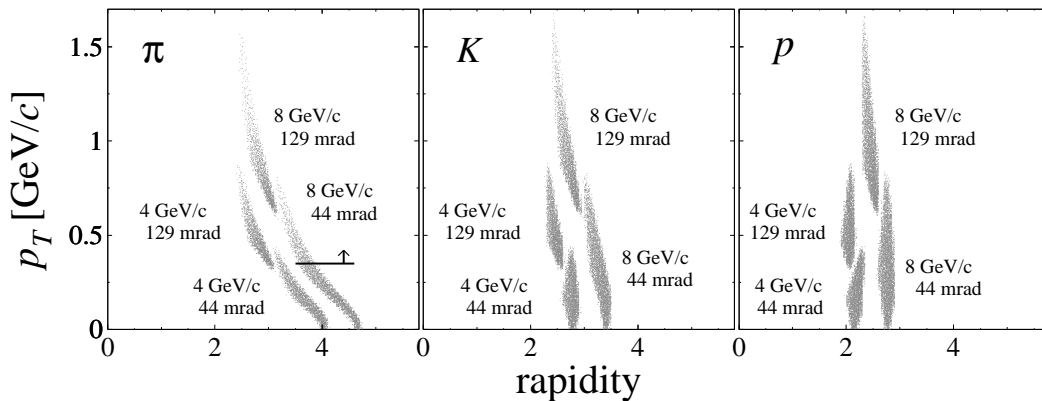


FIG. 2: The  $\pi$ ,  $K$ , and  $p$  acceptance in rapidity and  $p_T$ . In this analysis, pions at the 8 GeV/c 44 mrad angle setting are selected in  $p_T > 0.35$  MeV/c.

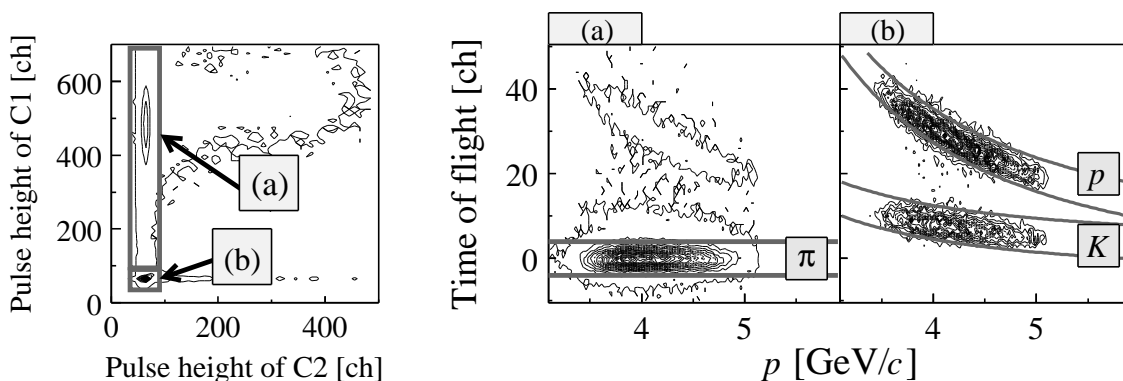


FIG. 3: An example of particle identification in the 4 GeV/c setting. The contour plot shows pulse heights of C1 and C2 (left). The region (a) is electron veto and pion required by C1 and C2 pulse heights. The region (b) is electron and pion veto by C1 and C2. The regions (a) and (b) in right plot correspond to the left plots. The pair of plots on the right are TOF at H3 as a function of momentum with C1 and C2 cuts. The curves show  $\pm 2.5$  sigma of TOF resolution from the peak. Particles between the curves are selected.

Two angular settings, 44 mrad and 129 mrad provided the range in transverse momentum ( $p_T$ ). Combining these settings yields transverse momenta from  $p_T = 0$  to 0.9 GeV/c (0 to 1.6 GeV/c) for 4 GeV/c (8 GeV/c) setting. Figure 2 shows the NA44 acceptance in  $p_T$  and rapidity for  $\pi$ ,  $K$ , and  $p$ . The NA44 acceptance includes mid-rapidity ( $y_{mid}=2.9$ ) for Pb+Pb collisions at 158 GeV/c per nucleon.

The invariant cross section was produced by the following analysis procedures: track and momentum reconstruction, particle identification of tracks, a selection of high multiplicity events, an acceptance correction via a Monte-Carlo simulation, normalization by summing of beam scalers, and multiplicative correction factors for cuts.

The hit positions on PC, H2, H3, SC1, and SC2 were used to reconstruct tracks by fitting them with a straight line using the  $\chi^2$ -minimization method. As is clear from Fig. 1, the tracking detectors lie outside the magnetic field. The momentum resolution  $\delta p/p$  is 0.2% for all particle species.

TABLE I: The number of particles selected by the cuts for each spectrometer setting. The event fraction is  $3.7 \pm 0.1\%$ .

nominal momentum [GeV/c]	angle [mrad]	particle species					
		$\pi^+$	$\pi^-$	$K^+$	$K^-$	$p$	$\bar{p}$
4 GeV/c	44	2713	3839	5150	5814	3644	428
	129	11498	11163	4238	12222	6577	1663
8 GeV/c	44	1272	992	14689	12563	6215	711
	129	5915	6785	22614	26578	41682	5834

Particle identification uses a combination of pulse heights in C1 and C2 with time-of-flight from CX to the hodoscopes. In the 4 GeV/c spectrometer setting, pions are separated from  $K$  and  $p$  by C1 and C2, and then  $K/p$  separation is done by TOF. In the 8 GeV/c setting,  $e$  and  $\pi$  are vetoed by C2, and then  $K/p$  separation is done by C1. For pions from 8 GeV/c setting the contamination from electrons is negligible for  $p_T > 0.35$  MeV/c.

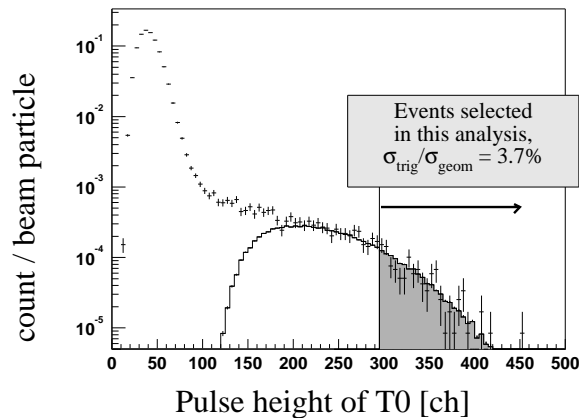


FIG. 4: The pulse height distribution of scintillation multiplicity counter. The scatter plot is from valid beam run. Events with a trigger required a pulse height in the counter are shown by the solid line histogram. The hatched region is used for the analysis.

The statistics of each particle are shown in Table I.

H3 provides the primary TOF information because of the longer flight path to H3. The timing resolution of H3 is better than H2. Figure 3 shows an example of particle identification in the 4 GeV/c setting. The left-hand side shows a scatter plot of pulse heights in C1 and C2. Events containing an electron fire C2, and are rejected by requiring minimal in C2 pulse height. Regions (a) and (b) in the plots of TOF as a function of momentum (right-hand figures) show the same events indicated in the left-hand side plot. Particles are selected via the bands shown by the curves in the figure. The contamination for each particle species is less than 3% in both momentum settings.

Central collisions are identified by the scintillation multiplicity counter, T0. Figure 4 shows the pulse height distribution from T0, with the scatter plot is corresponding to valid beam events. The solid line shows high multiplicity events selected by the trigger threshold on T0. The hatched region is used in the analysis. It is necessary to determine what fraction of all interactions satisfies the T0 threshold; this fraction is denoted by  $\lambda$ . The value of  $\lambda$  is obtained by scaling of the interaction probability of  $p$ +Pb collisions to one of Pb+Pb collision by a geometry factor of 2.9. The total Pb interaction probability is 3.4% for 2 mm Pb target. The events selected in the hatched region in Fig. 4 are the top  $3.7 \pm 0.1\%$  (statistical only) of these interactions. The region corresponds to average impact parameter  $\langle b \rangle \approx 5$  fm that is estimated by applying T0 acceptance cut to multiplicity in RQMD (v2.3) [8].

### III. ANALYSIS

In order to construct the invariant cross section, the effect of the acceptance is estimated by a Monte-Carlo

(MC) simulation based on TURTLE [9], which passes generated particle tracks through the detectors. The acceptance, reconstruction efficiencies, momentum resolution, and loss of pions and kaons due to in-flight-decays are estimated by comparing generated tracks with reconstructed tracks. The momentum spectrum and rapidity distribution for each particle species in Pb+Pb was taken from RQMD (v2.3), which has been shown to reproduce measured hadron distributions. The Monte-Carlo events were analyzed with the tracking programs exactly as applied to the physics events. The corrections are given by the ratio of the generated yield to the reconstructed yield as a function of  $m_T$  inside the rapidity acceptance. The absolute cross section as a function of  $m_T$  in a rapidity range  $\Delta y$  is given by

$$\begin{aligned} \frac{1}{\sigma} \frac{Ed^3\sigma}{dp^3} \Big|_{\Delta y} &= \frac{1}{N_{\text{event}}} \frac{1}{2\pi} \frac{dN}{m_T dm_T \Delta y} \\ &= \frac{1}{N_{\text{event}}} \frac{dn}{dm_T \Delta y} \times \frac{\frac{1}{2\pi} \frac{1}{m_T} \frac{d\check{n}_{mc}}{dm_T \Delta y}}{\frac{d\check{n}_r}{dm_T \Delta y}} \end{aligned}$$

where  $n$  is the number of measured tracks,  $N_{\text{event}}$  is the number of collisions,  $\check{n}_{mc}$  is the number of particles as input of the MC simulation and  $\check{n}_r$  is the number of tracks reconstructed in the simulation.

An effect of secondary hadronic interactions of produced protons and antiprotons in the spectrometer material was studied in a previous NA44 paper Ref. [1]. That effect does not distort the shape of the momentum distributions but reduces the yield. The correction factors to recover the lost fluxes were obtained to be 1.11 for protons and 1.17 for antiprotons, respectively.

The corrected momentum distribution is then normalized by using the number of beam particles, the interaction probability, the fraction of interactions satisfying the trigger, the measured live time of the data-acquisition system, and losses due to the cut for particle identification.

Separation of protons and kaons from pions is done via Cherenkov veto, but in the process some protons and kaons are rejected in events that also include a pion. The veto factor (i.e., the correction for this loss) for each particle and momentum setting is estimated by comparing the number of the particle with no Cherenkov veto to the number of particle with Cherenkov veto, using real data without Cherenkov veto. Since the veto factor depends on relative particle ratios in spectrometer, it must be independently estimated for each momentum and angle setting.

The transverse mass distribution is obtained from the two angle settings (44 mrad and 129 mrad). The data at 129 mrad have smaller (typically one half to one third) systematic errors in the absolute normalization than those at 44 mrad. Therefore, in this analysis, the data at 44 mrad were scaled to match those at 129 mrad in the  $m_T$  region where they overlap. The distributions from both settings were fit by exponentials with the same inverse slope parameter. An additional normalization

factor forces the 44 mrad setting match.  $dN/dy$  is the sum of the normalized cross section in each measured  $m_T$  bin plus integration of the fitted exponential distribution beyond the measurement region.

#### IV. SYSTEMATIC ERRORS

The inverse slope parameters are extracted by fitting the experimental distribution with a single  $m_T$  exponential function. Systematic errors on the inverse slope parameters are estimated by dividing the data into two  $p_T$  range for the fits. The systematic errors are shown with the inverse slope parameters in Table II.

The absolute normalization procedure results in significant uncertainties in  $dN/dy$ . Contributions include uncertainties on the following; the data-acquisition live time (5%), the stability of T0 pulse height to select event fraction (2%), the Cherenkov veto factor (<5%), the correction for particle loss due to quality cuts (<5%), and the extrapolation beyond the measurement region (<1~18%). The last three vary with particle species and spectrometer setting. Assuming the errors are uncorrelated, the total systematic error is obtained by adding the contributions in quadrature. The errors for each particle species and setting are shown with results in Table II.

#### V. FEED-DOWN FROM WEAK DECAYS

NA44 has no vertex detectors in the target region, therefore decay protons from some fraction of the short-lived particles such as strange baryons will be detected as protons in the spectrometer. This contamination of protons and antiprotons is not negligible.

The same Monte-Carlo used for acceptance corrections was also used to estimate the weak decay yields from  $\Lambda$ ,  $\Sigma^+$  and  $\Sigma^0$ . Since the lifetime of  $\Sigma^0$  is short, its yield was included into the  $\Lambda$  yield. The  $dN/dy$  for various particles near mid-rapidity in central collisions was taken from RQMD(v2.3).

The correction factor as a function of  $m_T$  is

$$C_p(m_T) = \frac{N_{p_{orig}}(m_T)}{N_{p_{orig}}(m_T) + N_{p_\Lambda}(m_T) + N_{p_\Sigma}(m_T)}$$

where  $N_{p_{orig}}$ ,  $N_{p_\Lambda}$  and  $N_{p_\Sigma}$  are the number of protons measured in NA44 spectrometer. The suffixes indicated origin of protons; original protons, protons from  $\Lambda$  decays and  $\Sigma^+$  decays, respectively. Figure 5 shows the correction factors as a function of  $m_T$ -mass. Since these depend on the ratio of  $\Lambda$  and  $\Sigma^+$  to proton, the production ratios were varied. The squares are the correction factor estimated from  $\Lambda/p$  and  $\Sigma/p$  ratios of RQMD, while the other curves assume yield ratios larger or smaller by a factor 1.5.

The correction procedure contributes to the systematic uncertainties on the inverse slopes of proton and antiproton by about 7% for the 4 GeV/ $c$  setting and about 3%

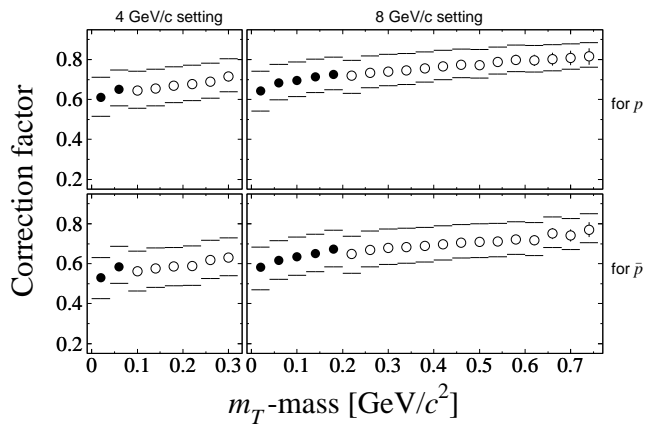


FIG. 5: The correction factors for proton and anti-proton as a function of  $m_T$ -mass. The solid (open) square corresponds to 44 (129) mrad setting. A detailed explanation of the figures is in the text.

for the 8 GeV/ $c$  setting. The errors due to feed-down correction on  $dN/dy$  are approximately 15% for protons and 19% for antiprotons in both 4 GeV/ $c$  and 8 GeV/ $c$  setting.

#### VI. RESULTS

The invariant cross sections measured in the NA44 spectrometer in Pb+Pb collisions are shown in Fig. 6. They are plotted as a function of  $m_T$  in the specified rapidity regions. The  $m_T$  distribution is generally well described at these energies by

$$\frac{1}{\sigma_{trig}} \frac{Ed^3\sigma}{dp^3} = Ae^{-(m_T-m)/T},$$

where  $A$  is a constant and  $T$  is the inverse slope parameter. Table II lists the inverse slope parameters, its fit region, and the values of  $dN/dy$ .

The slope parameters are consistent with previous NA44 results (Ref. [10]) within errors. The proton  $dN/dy$  in Pb+Pb collisions is reported with consistent values in Ref. [11]. The statistics in our previous publication are 1/3 to 3/4 of the statistics used in this paper. We note that the NA44 collaboration published a paper on pion and kaon spectra focusing on “strangeness enhancement” [3]. This analysis used a different definition of event fraction, which used the silicon multiplicity counter. The results are consistent within errors.

The NA49 collaboration has reported  $dN/dy$  distributions of  $\pi^+$ ,  $\pi^-$ ,  $K^+$ ,  $K^-$ ,  $p$ , and  $\bar{p}$  for the 5% most central Pb+Pb reactions [12, 13]. These values are higher than our data (top 3.7% event fraction). Their selection of events is, however, different from NA44. The top 5% NA49 data corresponds to mean impact parameter  $\langle b \rangle = 2.2$  fm [14]. On the other hand, the NA44 data corresponds to  $\langle b \rangle \approx 5$  fm. Comparing similar impact pa-

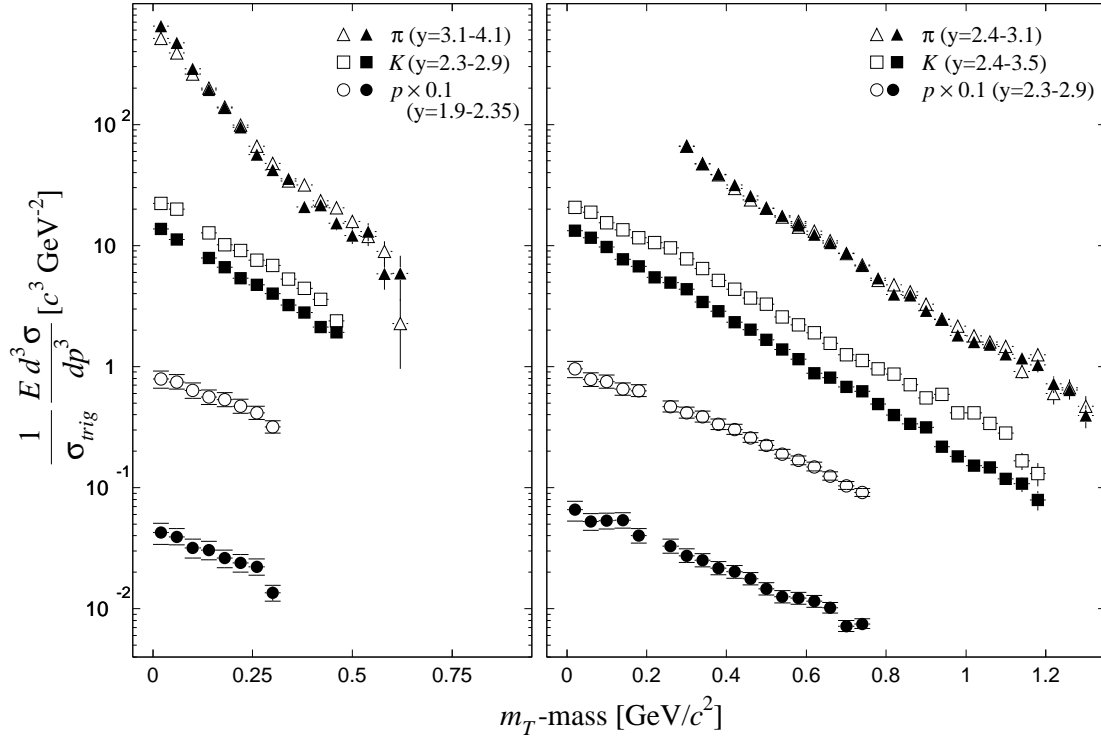


FIG. 6: Invariant cross section of  $\pi$ ,  $K$ , and  $p$  in Pb+Pb collisions as a function of  $m_T$ -mass. The open (solid) marker shows positive (negative) charged particle. The rapidity range for each particle is shown in the figure. The feed-down effect is corrected in proton and antiproton distributions. The horizontal bars above and below each point show systematic errors from the feed-down correction and correspond to the horizontal bars in Fig. 5. Note that the proton and anti-proton are scaled a factor 0.1 in the vertical direction.

TABLE II: The inverse slope parameters and  $dN/dy$  with statistical error (first) and systematic error (second). The pion  $dN/dy$  is obtained from the data of 4 GeV/ $c$  and 8 GeV/ $c$  setting at both 44 mrad and 129 mrad. The values for proton and antiproton including the feed-down correction are shown as  $p_c$  and  $\bar{p}_c$  and systematic errors include errors from feed-down correction.

	rapidity	Fit range $m_T$ -mass [GeV/ $c^2$ ]	Inverse slope [MeV/ $c^2$ ]	$dN/dy$
$\pi^+$	2.4-3.1	0.28-1.20	$207 \pm 3 \pm_2^3$	$150 \pm 3 \pm 8$
	3.1-4.1	0.00-0.56	$126 \pm 2 \pm_8^{55}$	
	2.4-4.1			
$\pi^-$	2.4-3.1	0.28-1.20	$201 \pm 3 \pm_1^2$	$162 \pm 2 \pm 10$
	3.1-4.1	0.00-0.56	$109 \pm 2 \pm_7^{50}$	
	2.4-4.1			
$K^+$	2.3-2.9	0.00-0.32	$221 \pm 9 \pm_2^{10}$	$24.0 \pm 0.2 \pm 2.1$
	2.4-3.5	0.00-0.84	$246 \pm 2 \pm_1^8$	
$K^-$	2.3-2.9	0.00-0.32	$224 \pm 7 \pm 1$	$14.8 \pm 0.5 \pm 1.1$
	2.4-3.5	0.00-0.84	$228 \pm 2 \pm_1^2$	
$p$	1.9-2.35	0.00-0.28	$319 \pm 23 \pm_1^{18}$	$33.3 \pm 0.8 \pm 4.0$
	2.3-2.9	0.00-0.68	$296 \pm 5 \pm_7^{17}$	
$\bar{p}$	1.9-2.35	0.00-0.28	$303 \pm 35 \pm_7^{34}$	$1.74 \pm 0.01 \pm 0.33$
	2.3-2.9	0.00-0.68	$300 \pm 9 \pm_1^7$	
$p_c$	1.9-2.35	0.00-0.28	$379 \pm 33 \pm_3^{28}$	$27.3 \pm 0.5 \pm 5.2$
	2.3-2.9	0.00-0.68	$327 \pm 6 \pm_{10}^{28}$	
$\bar{p}_c$	1.9-2.35	0.00-0.28	$360 \pm 53 \pm_{15}^{47}$	$1.43 \pm 0.04 \pm 0.39$
	2.3-2.9	0.00-0.68	$333 \pm 12 \pm_6^{10}$	

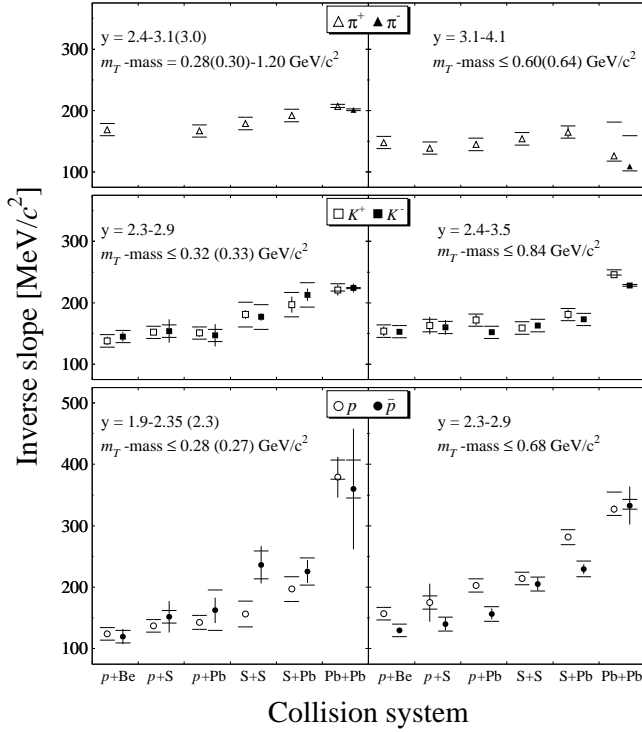


FIG. 7: Collision system dependence of charged pion, kaon, and proton inverse slope parameters. The slopes in  $p+A$  and  $S+A$  collisions are from Ref. [1, 2]. The  $m_T$  and rapidity values in parenthesis are for  $p+A$  and  $S+A$  collisions. Statistical errors and systematic errors are shown as vertical and horizontal bars above and below each point, respectively.

parameter regions,  $p-\bar{p}$  and  $\bar{p}$  are consistent with the recent NA49 results of Refs. [14, 15] within the errors.

We have obtained the invariant cross section of pions, kaons, and protons in  $Pb+Pb$  collisions using data analysis procedures compatible with these used in Refs. [1, 2]. Consequently, we can study the systematics of particle yields at CERN-SPS energy for many collision systems (450 GeV/c  $p+A$ , 200 A GeV/c  $S+A$ , and 158 A GeV/c  $Pb+Pb$ ).

Figure 7 shows the collision system dependence of inverse slope parameters for pions, kaons, and protons. The inverse slope of the pion distribution in  $0.3 < m_T - \text{mass} < 1.2 \text{ GeV}/c^2$  is increasing with collision system. On the other hand, the slope in the region  $m_T - \text{mass} < 0.6 \text{ GeV}/c^2$  in  $Pb+Pb$  is similar to one in  $p+A$  and  $S+A$  collision systems. However, the systematic error on the slope parameter for pions in the low  $p_T$  region is larger than in  $p+A$  and  $S+A$ , reflecting larger enhancement of pions at low  $p_T$ .

The kaon inverse slope parameters increase with collision system size slowly, but more rapidly than the pion inverse slope parameters. The proton inverse slopes are higher at mid-rapidity ( $y=2.3-2.9$ ) than at more backward rapidities ( $y=1.9-2.3$ ) in  $p+A$  and  $S+Pb$  collisions.

Figure 8 shows the collision system dependence of pion yields. The pion rapidity density in  $Pb+Pb$  collisions

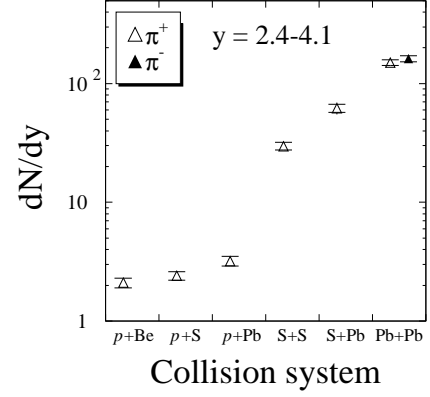


FIG. 8: Collision system dependence of charged pion  $dN/dy$ . The values of  $dN/dy$  in  $p+A$  and  $S+A$  collisions are from Ref. [2]. Statistical errors are hidden by the marker. Systematic errors are shown as horizontal bars above and below each point.

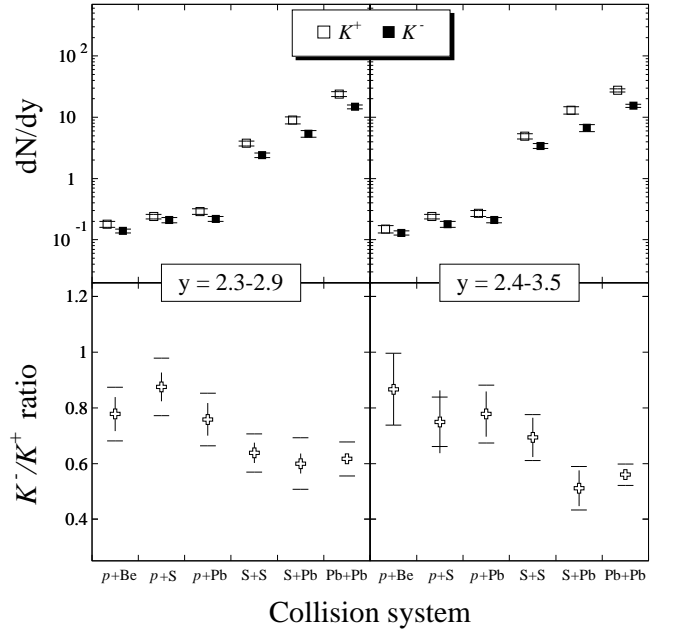


FIG. 9: Collision system dependence of charged kaon  $dN/dy$  and  $K^-/K^+$  ratio. The values of  $dN/dy$  in  $p+A$  and  $S+A$  collisions are from Ref. [2]. Statistical errors and systematic errors are shown as vertical and horizontal bars above and below each point, respectively.

increases by a factor of  $71 \pm 10$  compared to  $p+Be$  and  $5.1 \pm 0.6$  over  $S+S$ .  $dN/dy$  for  $\pi^-$  and  $\pi^+$  is comparable, within the errors.

Yields of  $K^+$  and  $K^-$ , and the  $K^-/K^+$  ratio are shown as a function of collision system in Fig. 9. The mid-rapidity  $dN/dy$  of  $K^+$  ( $K^-$ ) in  $Pb+Pb$  collisions increases by a factor of  $133 \pm 20$  ( $105 \pm 10$ ) compared to  $p+Be$  and  $6.4 \pm 0.9$  ( $6.2 \pm 0.8$ ) compared  $S+S$  collisions. The system size dependence is stronger than for pions, i.e., the  $K/\pi$  ratio increases from  $p+Be$  to  $Pb+Pb$ .

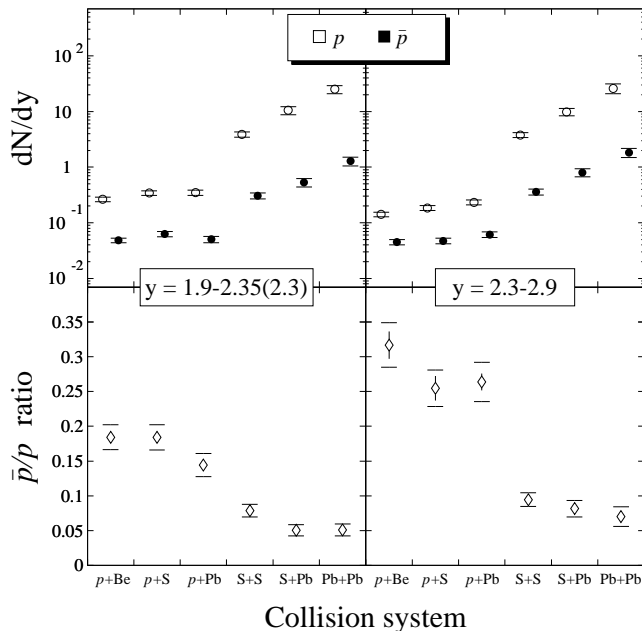


FIG. 10: Collision system dependence of proton and antiproton  $dN/dy$  (corrected for feed-down) and  $\bar{p}/p$  ratio. The values of  $dN/dy$  in  $p+A$  and  $S+A$  collisions are from Ref. [1]. Statistical errors and systematic errors are shown as vertical and horizontal bars above and below each point, respectively.

Figure 10 shows the system size dependence of  $dN/dy$  for protons and antiprotons. At mid-rapidity, the  $p$  ( $\bar{p}$ ) yield in Pb+Pb collisions increases by a factor of  $183 \pm 42$  ( $41 \pm 10$ ) compared to  $p+Be$ , and  $6.9 \pm 1.6$  ( $5.1 \pm 1.2$ ) compared to S+S collisions; proton  $dN/dy$  increases with system size more rapidly than antiprotons. In heavy ion collisions, the  $\bar{p}/p$  ratio decreases with system size (S+S to Pb+Pb), and falls more rapidly at mid-rapidity than at backward rapidity. This is exactly what is expected from increased stopping power, and therefore larger net baryon density, with larger colliding system size.

## VII. DISCUSSION

In heavy ion collisions, we use the notions of chemical freeze-out and thermal freeze-out to describe the moment when the inelastic interactions and elastic interactions stop, respectively. In this section, we will describe the parameters extracted from the measured spectra and yields.

### A. Transverse momentum distributions

The transverse momentum distributions of hadrons have been measured by several experimental groups at BNL-AGS and CERN-SPS including NA44 [10]. The  $m_T$  distributions are studied from the viewpoint of collective flow, with local thermal equilibrium at mid-rapidity

based on Refs. [16, 17]. The NA44 collaboration has reported a thermal freeze-out temperature  $T_{th} \approx 140$  MeV [10] in the collisions at the  $\sqrt{s_{NN}} \approx 18$  GeV. Recently two-pion interferometry results have been combined with single particle spectra to measure the transverse flow and thermal freeze-out temperature [12, 18]. These studies find  $T_{th} \approx 120$  MeV [12] and 100 MeV [18]. Evaluating those reports equally, one concludes that the thermal freeze-out temperature is in the range 100–140 MeV.

### B. Particle yields

At chemical freeze-out, the density of different particles can be characterized by macroscopic parameters; the chemical freeze-out temperature and chemical potentials. Here, we adopt a chemical freeze-out model based on Ref. [19], using the grand canonical ensemble. We assumed no difference between  $u$  and  $d$  quarks for the chemical potentials. Therefore, the hadron gas is described by chemical freeze-out temperature ( $T_{ch}$ ), light ( $u$  and  $d$ ) quarks potential ( $\mu_q$ ), strange quark potential ( $\mu_s$ ), and strangeness saturation factor  $\gamma_s$ . The density of a particle  $i$  in the hadron gas is given by:

$$\rho_i = \gamma_s^{\langle s+\bar{s} \rangle_i} \frac{g_i}{2\pi^2} T_{ch}^3 \left( \frac{m_i}{T_{ch}} \right)^2 K_2(m_i/T_{ch}) \lambda_q^{Q_i} \lambda_s^{s_i} \quad (1)$$

where  $m_i$  is the mass of the particle  $i$ ,  $g_i$  is a number of spin-isospin freedom,  $K_2$  is the second order modified Bessel function and

$$\lambda_q = \exp(\mu_q/T_{ch}), \quad \lambda_s = \exp(\mu_s/T_{ch}).$$

The potential  $\mu_q$  is for  $u/d/\bar{u}/\bar{d}$  quarks, and  $\mu_s$  is for  $s/\bar{s}$  quarks.  $Q_i$  corresponds to number of valence  $u/d$  quark contents of particle species  $i$  ( $Q_i = \langle u - \bar{u} + d - \bar{d} \rangle_i$ ), and  $s_i$  is for valence  $s$  quark contents ( $s_i = \langle s - \bar{s} \rangle_i$ ). The factor  $\gamma_s$  ( $0 \leq \gamma_s \leq 1$ ) is introduced to take account of possible incomplete chemical equilibrium for strange particles [20].  $\gamma_s=1$  signifies full strangeness chemical equilibrium. The power factor of  $\gamma_s$  is total number of  $s$  and  $\bar{s}$  quarks in the particle. Note that we use the Boltzmann approximation for all hadrons excepting pions and the Bose distribution is applied to pions. The particle densities are computed by Eq. (1) for the hadron gas including known resonances up to mass of 1.7 GeV/ $c^2$ , and the effect of broad resonance mass widths is taken into account [19]. The resonance decay to lower mass hadrons after chemical freeze-out is also taken into account. Therefore, the final particle densities for the pions, kaons, and protons are given by the sum of the direct production and the decays of the resonances. Here, we apply the above procedure for the particle yields observed near mid-rapidity by NA44 for  $p+A$ ,  $S+A$ , and  $Pb+Pb$  collisions [1, 2].

Table III lists the fit results of the chemical freeze-out parameters  $T_{ch}$ ,  $\mu_q$ ,  $\mu_s$ , and  $\gamma_s$ . Those values are



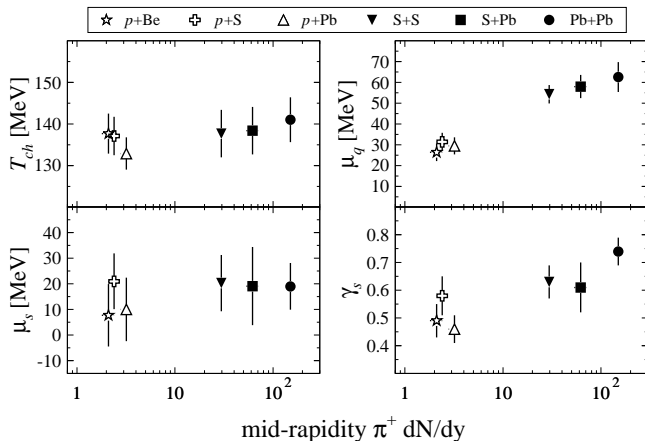


FIG. 11: Collision system dependence of the chemical freeze-out parameters.

TABLE III: The macroscopic parameters for the description of the chemical freeze-out near central rapidity for Pb+Pb, S+Pb, and  $p$ +A collisions from the NA44 data. The values of  $dN/dy$  from Refs. [1, 2] are used to obtain the parameters in the  $p$ +A and S+A collisions.

	$T_{ch}$ [MeV]	$\mu_q$ [MeV]	$\mu_s$ [MeV]	$\gamma_s$
Pb+Pb	$141 \pm 5$	$63 \pm 7$	$19 \pm 9$	$0.74 \pm 0.05$
S+Pb	$139 \pm 6$	$58 \pm 6$	$19 \pm 15$	$0.61 \pm 0.09$
S+S	$138 \pm 4$	$54 \pm 4$	$20 \pm 11$	$0.63 \pm 0.06$
$p$ +Pb	$133 \pm 4$	$30 \pm 4$	$10 \pm 12$	$0.46 \pm 0.05$
$p$ +S	$137 \pm 5$	$31 \pm 4$	$21 \pm 11$	$0.58 \pm 0.07$
$p$ +Be	$138 \pm 5$	$26 \pm 4$	$8 \pm 12$	$0.49 \pm 0.06$

obtained by fitting the procedure described in this section to the data, using MINUIT [21] for  $\chi^2$ -minimization. Figure 11 shows the collision system dependence of the parameters. The chemical freeze-out temperatures ( $T_{ch}$ ) are approximately 140 MeV in  $p$ +Be through Pb+Pb collisions; within error, there is no dependence on system size. Comparing to the other results, the  $T_{ch}$  is consistent with Ref. [22] ( $T_{ch}=133$ –144 MeV) and smaller than Ref. [23] ( $T_{ch}=158 \pm 3$  MeV) and Ref. [24] ( $T_{ch}=168 \pm 2.4$  MeV). As reported in Refs. [19, 25] there is a rapidity dependence of chemical freeze-out parameters. Those results show that a lower value of the temperature is obtained when only mid-rapidity data are used. The values of  $\mu_q$  increases with the size of the collision system. The limited number of particle species used in this analysis may also influence the value of  $T_{ch}$ . Since the chemical freeze-out temperature is independent of collision systems ( $p$ +A and A+A), the system in  $p$ +A collisions has smaller  $\mu_q/T_{ch}$ , that is, smaller baryon density than A+A collisions.  $\mu_s$  is 10–20 MeV for  $p$ +A through Pb+Pb.  $\mu_s$  should be zero in a equilibrated quark gluon plasma and on the phase boundary of hadron gas [20, 26, 27]. Consequently, the small value we obtain may suggest that chemical freeze-out takes place near the phase transition.

In addition, we observed that the values of strangeness saturation factor  $\gamma_s$  are smaller than unity for all collisions. This indicates that the hadron gas has not reached full chemical equilibrium for strange particles in heavy ion collisions in the CERN-SPS energy region. On the other hand, the value of  $\gamma_s$  increases with collision system size, e.g., the value of  $\gamma_s$  is higher in heavy ion collisions than those from  $p$ +A collisions. The use of the grand canonical ensemble for analysis of strange particle production in  $p$ +A collisions does not take into account phase space effects arising from production of  $s$  and  $\bar{s}$  pairs. Consequently,  $\gamma_s$  is expected to be lower than in heavy ion collisions where more strange quark pairs are produced [28, 29].

It should be pointed out that the model applied assumes all hadrons are in chemical equilibrium. The nature of the equilibration is not clear; it could be reached by re-scatterings among constituents or merely by filling the phase space. In addition, the multi-strange baryons might be out of equilibrium [19, 22, 30]. As described in Refs. [23, 31], the chemical freeze-out model can generally describe hadron ratios well even with a small number of ratios. We note that the system is not necessarily in global equilibration over full rapidity range because particles can interact only in a subset of the system due to rapid longitudinal expansion. Additionally, the homogeneity length measured by two-particle correlations supports that the equilibration occurs in a limited phase space [32]. It is reasonable, though to use the chemical freeze-out model to describe ratios at mid rapidity [33].

## VIII. CONCLUSION

The NA44 experiment has measured single particle distributions for charged pions, kaons, and protons as functions of transverse mass ( $m_T$ ) near mid-rapidity in 158 A GeV/c Pb+Pb collisions. We studied particle ratios near mid-rapidity region from the viewpoint of chemical freeze-out for  $p$ +A (A = Be, S, Pb), S+A (A = S, Pb), and Pb+Pb collisions. It is found that chemical freeze-out of mid-rapidity particles occurs at a temperature of  $\approx 140$  MeV for all collisions. The values of the light quark chemical potential ( $\mu_q$ ) are approximately 30 MeV in  $p$ +A and 54 to 63 MeV in S+S to Pb+Pb collisions. The trend of  $\mu_q$  shows that the baryon stopping power increases with collision system size. The values of the strange quark chemical potential are about 10 to 20 MeV. The strangeness saturation factor is 0.61 to 0.75 in heavy ion collisions and 0.46 to 0.58 in  $p$ +A, indicating that  $p$ +A collisions are further away from strangeness equilibration than A+A collisions.

## Acknowledgments

The NA44 collaboration wishes to thank the staff of the CERN PS-SPS accelerator complex for their excel-

lent work. We are also grateful for support given by the Danish Natural Science Research Council; the Japanese Society for the Promotion of Science; the Ministry of Education, Science and Culture, Japan; the Swedish Sci-

ence Research Council; the Austrian Fond für Förderung der Wissenschaftlichen Forschung; the National Science Foundation, and the US Department of Energy.

- 
- [1] I. G. Bearden *et al.* (NA44), Phys. Rev. C **57**, 837 (1998).  
 [2] H. Bøggild *et al.* (NA44), Phys. Rev. C **59**, 328 (1999).  
 [3] I. Bearden *et al.* (NA44), Phys. Lett. B **471**, 6 (1999).  
 [4] I. G. Bearden *et al.* (NA44), Phys. Rev. Lett. **85**, 2681 (2000).  
 [5] H. Bøggild *et al.* (NA44), Phys. Lett. B **302**, 510 (1993).  
 [6] N. Maeda *et al.*, Nucl. Instrum. Methods A **346**, 132 (1994).  
 [7] T. Kobayashi and T. Sugitate, Nucl. Instrum. Methods A **287**, 389 (1990).  
 [8] H. Sorge, Phys. Rev. C **52**, 3291 (1995).  
 [9] *CN/ASD, Beam Transport Simulation, Including Decay W151.*, CERN, Geneva (1974).  
 [10] I. G. Bearden *et al.* (NA44), Phys. Rev. Lett. **78**, 2080 (1997).  
 [11] I. G. Bearden *et al.* (NA44), Phys. Lett. B **388**, 431 (1996).  
 [12] H. Appelshäuser *et al.* (NA49), Phys. Rev. Lett. **82**, 2471 (1999).  
 [13] F. Siklér (for the NA49 collaboration), Nucl. Phys. A **661**, 45c (1999).  
 [14] G. E. Cooper (for the NA49 collaboration), Nucl. Phys. A **661**, 362c (1999).  
 [15] G. I. Veres (for the NA49 collaboration), Nucl. Phys. A **661**, 383c (1999).  
 [16] E. Schnedermann, J. Sollfrank, and U. Heinz, Phys. Rev. C **48**, 2462 (1993).  
 [17] T. Cörge and B. Lörstad, Phys. Rev. C **54**, 1390 (1996).  
 [18] J. Rayford Nix, Phys. Rev. C **58**, 2303 (1998).  
 [19] J. Sollfrank, U. Heinz, H. Sorge, and N. Xu, Phys. Rev. C **59**, 1637 (1999).  
 [20] J. Rafelski, Phys. Lett. B **262**, 333 (1991).  
 [21] F. James, *MINUIT - Function Minimization and Error Analysis. Reference Manual*, CERN, Geneva (1984).  
 [22] J. Letessier and J. Rafelski, J. Phys. G. **25**, 295 (1999).  
 [23] F. Becattini, J. Cleymans, A. Keränen, E. Suhonen, and K. Redlich, Phys. Rev. C **64**, 024901 (2001).  
 [24] P. Braun-Munzinger, I. Heppe, and J. Stachel, Phys. Lett. B **465**, 15 (1999).  
 [25] M. Kaneta and N. Xu, J. Phys. G. **27**, 589 (2001).  
 [26] K. S. Lee, M. J. Rhoades-Brown, and U. Heinz, Phys. Rev. C **37**, 1452 (1988).  
 [27] M. N. Asprouli and A. D. Panagioutou, Phys. Rev. D **51**, 1086 (1995).  
 [28] K. Redlich, S. Hamieh, and A. Tounsi, J. Phys. G. **27**, 413 (2001).  
 [29] K. Redlich, Nucl. Phys. A **698**, 94 (2002).  
 [30] H. van Hecke, H. Sorge, and N. Xu, Phys. Rev. Lett. **81**, 5764 (1998).  
 [31] J. Cleymans, H. Oeschler, and K. Redlich, Phys. Rev. C **59**, 1663 (1999).  
 [32] U. Heinz and B. V. Jacak, Ann. Rev. Nucl. Part. Sci. **49**, 529 (1999).  
 [33] J. Cleymans, H. Oeschler, and K. Redlich, J. Phys. G. **25**, 281 (1999).